Department of Information Technology and Mathematical Methods

Working Paper

Series "*Mathematics and Statistics*"

Numerical solution of flow rate boundary problems
for an incompressible fluid in deformable domains

by

Luca Formaggia, Alessandro Veneziani, Christian Vergara

Numerical solution of flow rate boundary problems for an incompressible fluid in deformable domains

Luca Formaggia

MOX, Dipartimento di Matematica, Politecnico di Milano, Piazza L. Da Vinci 32, 20133 Milano, Italy - `luca.formaggia@polimi.it`

Alessandro Veneziani

Dept. of Mathematics and Computer Science, Emory University, Atlanta, GA, USA, `ale@mathcs.emory.edu`

Christian Vergara

Dept. of Information Technology and Mathematical Methods, Università degli Studi di Bergamo, Viale Marconi 5, 24044 Dalmine (BG), Italy - `christian.vergara@unibg.it`

Abstract

In this paper we consider the numerical solution of the interaction of an incompressible fluid and an elastic structure in a truncated computational domain. As well known, in this case there is the problem of prescribing realistic boundary data on the artificial sections, when only partial data are available. This problem has been investigated extensively for the rigid case. In this work we start considering the compliant case, by focusing on the flow rate conditions for the fluid. We propose three formulations of this problem, different algorithms for its numerical solution and carry out several 2D numerical simulations with the aim of comparing the performances of the different algorithms.

Key words: Fluid-structure interaction, flow rate conditions, haemodynamics.

1 Introduction

Numerical simulations of incompressible flows in network of pipes almost invariably require to bound the domain of interest with artificial boundaries that
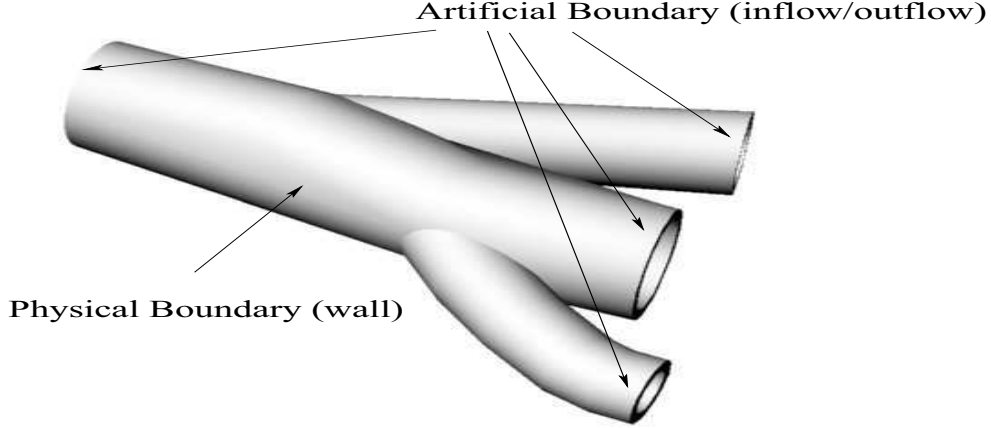
Fig. 1. Example of truncated computational domain

interfaces it with the entire network (see Fig. 1). Unfortunately, no physical arguments can be invoked for the prescription of conditions on these boundaries. Data can be prescribed from available measures. In some applications these measures are not enough for the well-posedness of the fluid problem. A typical example of interest in the present work is when flow rate in a pipe is measured, which is quite typical in haemodynamics. Flow rate is the average value of the normal velocity (multiplied by the fluid density) through the artificial section. Mathematical problem would require instead a pointwise data set for the velocity (Dirichlet conditions). Practical approaches for overcoming the under-determination are based on the selection of a realistic velocity shape fitting the measured flow rate. Despite of its simplicity, this approach introduces a strong bias in the numerical simulation. In [13] the problem of artificial boundaries and flow rate problems has been investigated with a more mathematically sound approach, resorting to the selection of a suitable variational formulation of the problem at hand. Homogeneous conditions natural for the selected variational formulation complete the defective data. For the flow rate problem, however, this approach requires the introduction of non-standard functional spaces, not straightforwardly prone to numerical discretization. Alternative approaches have been proposed in the last years, see [10,18,19,12]. A complete introduction to these topics can be found in [11], Chap. 11, in the context of geometrical multiscale models for the circulation. Computational haemodynamics is the application that has mainly (even if not exclusively) driven the present research. In this context, a complete description of the problem includes the compliance of the walls (Fluid Structure Interaction - FSI - problems). Artificial boundaries should be considered not only for the fluid but also for the structure problem. Specific mathematical and numerical appropriate techniques should be devised for the reliable solution to fluid-structure interaction problems with defective boundary data both for the fluid and the structure problems (see [11]). This paper is a first step in this direction. More precisely, we consider the fluid problem with flow rate conditions. We assume here that the structure problem features a complete

2

set of boundary conditions. In a forthcoming paper we will consider the case where both fluid and structure have defective boundary data on the artificial sections.

The purpose of this paper is to devise and compare possible strategies by extending the different methods proposed for the rigid case. It is worth mentioning that some preliminary results have been proposed in [16] limitedly to one particular strategy and to the case of a membrane structure (i.e. a 2D structure coupled to a 3D fluid domain). Here we consider specifically methods working for thick 3D structures.

The outline of the paper is as follows. In Sect. 2 we introduce the mathematical formulation of the flow rate problem in compliant domains. In view of the methods introduced later on, we address a formulation where velocity matching condition between fluid and structures is forced in a weak sense. We analyze the well posedness of this formulation. In Sect. 3 we present a first class of possible methods, stemming from segregated procedures for the fluid-structure interaction solution. Actually in partitioning fluid and structure computations, at each step fluid is solved in a "frozen" domain, so that methods for the prescription of the flow rate proposed for the rigid case can be straightforwardly applied. However, both segregated methods and techniques for defective flow rate problems are based on iterative procedures, so a direct implementation of this approach leads to nested iterative methods, typically having high computational costs. Most specific techniques for the compliant case are introduced in Sect. 4 and 5. More precisely, in Sect. 4 we introduce a method based on the extension of the augmented formulation introduced in [10,18] to the whole flow-rate/FSI problem. In particular, we consider an algorithm based on an algebraic splitting of the augmented problem (see [18]), which has the practical feature of resorting to the solution of standard FSI problems, affordable, for example, by a commercial package even when used as *black-box* solvers. In Sect. 5, we recast the problem in terms of the minimization of an appropriate functional measuring the distance between the computed and the prescribed flow rates with the constraint of the fluid-structure interaction problem, extending the strategy proposed for the rigid case in [12]. In particular, we use the normal stress on the artificial boundaries as control variable for driving the minimization of the constrained functional. We present different methods for the solution of the minimization problem, with the aim of reducing the computational costs mainly by avoiding nested iterations. Sect. 6 is devoted to the numerical results. We present several test cases, comparing numerical efficiency of the proposed methods. Finally, in Sect. 7 we draw some conclusions.

3

2 The Fluid-Structure Interaction problem

2.1 General setting and weak formulation

Let us consider a truncated computational domain $\Omega^t \subset \mathbb{R}^d$ (d=2, 3, being the space dimension), with r artificial sections. This domain is divided into a sub-domain Ω_s^t occupied by an elastic structure and its complement Ω_f^t occupied by the fluid. The fluid-structure interface Σ^t is the common boundary between Ω_s^t and Ω_f^t (see Fig. 2), whilst with Γ_i^t and $\Gamma_{i,s}^t$ we denote the fluid and structure artificial sections. Furthermore, $\boldsymbol{n}$ is the outward normal on $\partial\Omega_f^t$. The initial configuration Ω^0 at $t = 0$ is considered as the reference one.
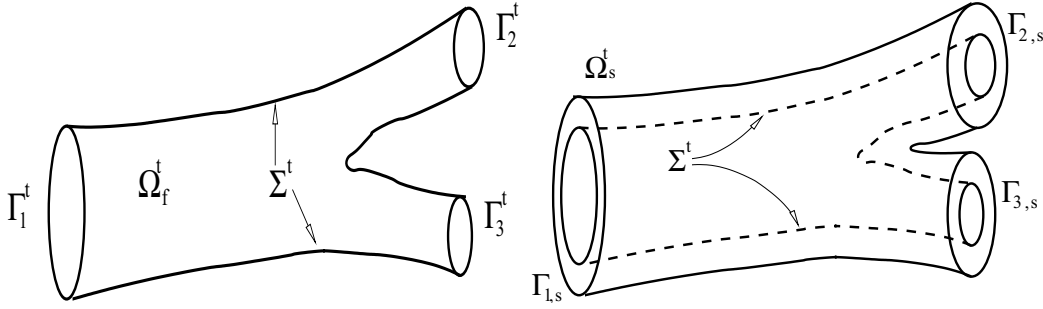

Fig. 2. Example of truncated computational fluid domain Ω_f^t (left) and solid domain Ω_s^t (right). In this picture $r = 3$.

We adopt a purely Lagrangian approach to describe the structure kinematics and then we refer always to the reference domain $\Omega_s := \Omega_s^0$. Hereafter, $\widehat{\boldsymbol{\eta}}$ denotes the displacement of the solid medium with respect to this configuration. For any function $\widehat{g}$ defined in the reference solid configuration, we denote by g its counterpart in the current domain. The solid is assumed to be a linear elastic material, characterized by the Cauchy stress tensor

$$\boldsymbol{T}_s(\boldsymbol{\eta}) = \lambda(\nabla \cdot \boldsymbol{\eta})\boldsymbol{I} + c(\nabla\boldsymbol{\eta} + (\nabla\boldsymbol{\eta})^T)$$

where λ and c are the Lamé constants and I is the identity tensor.

On the other hand, the fluid problem is stated in an *Arbitrary Lagrangian-Eulerian* (ALE) framework (see, e.g., [15,8]). The ALE mapping is defined by an appropriate lifting of the structure displacement. A classical choice is to consider a harmonic extension operator in the reference domain. In order to write the fluid problem according to the ALE formulation, we recall the definition of ALE time derivative of the velocity $\boldsymbol{u}$:

$$\frac{D^A\boldsymbol{u}}{Dt} = \frac{\partial\boldsymbol{u}}{\partial t} + \boldsymbol{w} \cdot \nabla\boldsymbol{u},$$

where $\partial \boldsymbol{u}/\partial t$ is the Eulerian derivative and $\boldsymbol{w}$ is the velocity of the points of the fluid domain defined by the ALE map. The fluid is assumed to be homogeneous, Newtonian and incompressible, with Cauchy stress tensor given by

$$\boldsymbol{T}_f(\boldsymbol{u}, p) = -p\boldsymbol{I} + \mu(\nabla \boldsymbol{u} + (\nabla \boldsymbol{u})^T),$$

where p is the pressure and μ the dynamic viscosity. Moreover, we collect the fluid artifical sections in three distinct subregions, namely $\Gamma_F^t := \bigcup_{i=1}^m \Gamma_i^t, m \leq r$, Γ_D^t and Γ_N^t, and the structure ones in two subregions, namely $\Gamma_{D,s}^0$ and $\Gamma_{N,s}^0$. Then, the complete problem in strong form reads:

(1) *Flow-rate/Fluid-structure problem.* Find the fluid velocity $\boldsymbol{u}$, pressure p and the structure displacement $\widehat{\boldsymbol{\eta}}$ such that

$$\begin{cases} \rho_f \frac{D^A \boldsymbol{u}}{Dt} + \rho_f((\boldsymbol{u} - \boldsymbol{w}) \cdot \nabla)\boldsymbol{u} - \nabla \cdot \boldsymbol{T}_f = \boldsymbol{f}_f & \text{in } \Omega_f^t \times (0, T), \\ \nabla \cdot \boldsymbol{u} = 0 & \text{in } \Omega_f^t \times (0, T), \\ \rho_s \frac{\partial^2 \widehat{\boldsymbol{\eta}}}{\partial t^2} - \nabla \cdot \widehat{\boldsymbol{T}}_s = \widehat{\boldsymbol{f}}_s & \text{in } \Omega_s^0 \times (0, T), \\ \boldsymbol{u} = \frac{\partial \boldsymbol{\eta}}{\partial t} & \text{on } \Sigma^t \times (0, T), \\ \boldsymbol{T}_s \boldsymbol{n} - \boldsymbol{T}_f \boldsymbol{n} = \boldsymbol{0} & \text{on } \Sigma^t \times (0, T), \\ \int_{\Gamma_i^t} \boldsymbol{u} \cdot \boldsymbol{n} \, d\gamma = F_i, \quad i = 1, \ldots, m & t \in (0, T). \end{cases} \tag{1}$$

(2) *Geometry problem.* Given the interface structure displacement $\boldsymbol{\eta}|_{\Sigma^t}$, find a map $\mathcal{A} : \Omega_f^0 \to \Omega_f^t$ through an harmonic extension Ext of this boundary value and find accordingly the new fluid domain Ω_f^t by moving the point $\boldsymbol{x}_0$ of the reference domain Ω_f^0:

$$\mathcal{A}^t(\boldsymbol{x}_0) = \boldsymbol{x}_0 + \text{Ext}(\widehat{\boldsymbol{\eta}}|_{\Sigma^0}), \quad \boldsymbol{w} = \partial_t \mathcal{A}^t \circ (\mathcal{A}^t)^{-1}, \quad \Omega_f^t = \mathcal{A}^t(\Omega_f^0).$$

Here, ρ_s is the structure density, $F_i, i = 1, \ldots, m$, are given functions of time and $\boldsymbol{f}_f$ and $\widehat{\boldsymbol{f}}_s$ the forcing terms. System (1) has to be endowed with suitable Dirichlet boundary conditions on Γ_D and $\Gamma_{D,s}$ and Neumann boundary conditions Γ_N and $\Gamma_{N,s}$. The partition between Dirichlet and Neumann boundaries can be different for the normal and the tangential direction of $\boldsymbol{u}$ and $\boldsymbol{\eta}$. Two transmission conditions are enforced at the interface: the *continuity of fluid and structure velocities* $(1)_4$ and the *continuity of stresses* $(1)_5$. The fluid and structure are also coupled by the geometry problem, leading to a highly non-linear system of partial differential equations. Finally, system (1) has to be endowed with suitable initial conditions.

2.2 Time discretization, weak formulation and treatment of the interface position

Let us now consider the time discretization and the weak formulation of system (1). Let Δt be the time step size and $t^n = n\Delta t$ for $n = 0, \ldots, N$. We denote by z^n the approximation of a time dependent function z at time level t^n. We consider a backward Euler scheme for the time discretization of the fluid problem and an implicit second order BDF scheme for the structure problem. Observe, however, that all the arguments detailed in this work can be extended to other time discretization schemes.

For the moment being, we consider the case $\Gamma_F^t = \emptyset$, that is no flow rate conditions are prescribed. Extension to the case of such conditions is presented later on.

In order to treat the nonlinearity given by the convective term and by the fluid domain, we consider the *semi-implicit* treatment (see e.g. [9,4,3]). Denote by Ω_f^*, $\boldsymbol{u}^*$ and $\boldsymbol{w}^*$ appropriate extrapolations of the fluid domain, fluid velocity and fluid domain velocity, respectively. The simplest choice is given by the first order extrapolations $\Omega_f^* = \Omega_f^n$, $\boldsymbol{u}^* = \boldsymbol{u}^n$ and $\boldsymbol{w}^* = \boldsymbol{w}^n$. More accurate extrapolations can be considered as well.

Let us introduce the following spaces:

$$\boldsymbol{V}^* = \{\boldsymbol{v} \in \boldsymbol{H}^1(\Omega_f^*) : \boldsymbol{v}|_{\Gamma_D^*} = \boldsymbol{0}\},$$
$$Q^* = L^2(\Omega_f^*),$$
$$\boldsymbol{W} = \{\widehat{\boldsymbol{\psi}} \in \boldsymbol{H}^1(\Omega_s^0) : \widehat{\boldsymbol{\psi}}_{\Gamma_{D,s}^0} = \boldsymbol{0}\}$$
$$\boldsymbol{Z}^* = \left\{(\boldsymbol{v}, \widehat{\boldsymbol{\psi}}) \in \boldsymbol{V}^* \times \boldsymbol{W} : \boldsymbol{v}|_{\Sigma^*} = \frac{\psi|_{\Sigma^*}}{\Delta t}\right\}.$$

Moreover, set

$$A(\boldsymbol{u}, \boldsymbol{\eta}; \boldsymbol{v}, \boldsymbol{\psi})^* := \frac{\rho_f}{\Delta t}(\boldsymbol{u}, \boldsymbol{v})_f^* + (\boldsymbol{T}_f, \nabla \boldsymbol{v})_f^* + \rho_f(((\boldsymbol{u}^* - \boldsymbol{w}^*) \cdot \nabla)\boldsymbol{u}, \boldsymbol{v})_f^* +$$

$$+ \rho_s\left(\frac{\widehat{\boldsymbol{\eta}}}{\Delta t^2}, \frac{\widehat{\boldsymbol{\psi}}}{\Delta t}\right)_s + \left(\widehat{\boldsymbol{T}}_s, \frac{1}{\Delta t}\nabla\widehat{\boldsymbol{\psi}}\right)_s$$

and

$$B(q; \boldsymbol{v}, \boldsymbol{\psi})^* = -(q, \nabla \cdot \boldsymbol{v})_f^*$$

where $(\boldsymbol{v}, \boldsymbol{w})_f^* := \int_{\Omega_f^*} \boldsymbol{v} \cdot \boldsymbol{w}\, d\boldsymbol{x}$ and $(\boldsymbol{\psi}, \boldsymbol{\chi})_s := \int_{\Omega_s^0} \boldsymbol{\psi} \cdot \boldsymbol{\chi}\, d\boldsymbol{x}$. Then, the weak formulation for the discretized-in time problem with a semi-implicit treatment reads as follows.

For each n we perform the following steps

1. Compute suitable extrapolations Ω_f^*, $\boldsymbol{u}^*$ and $\boldsymbol{w}^*$ of Ω_f^{n+1}, $\boldsymbol{u}^{n+1}$ and $\boldsymbol{w}^{n+1}$, respectively.
2. Given $\boldsymbol{f}_f^{n+1} \in L^2(\Omega_f^*)$ and $\widehat{\boldsymbol{f}}_s^{n+1} \in \boldsymbol{L}^2(\Omega_s^0)$, find $(\boldsymbol{u}^{n+1}, \widehat{\boldsymbol{\eta}}^{n+1}) \in \boldsymbol{Z}^*$ and $p^{n+1} \in Q^*$ such that

$$
\begin{cases}
A(\boldsymbol{u}^{n+1}, \boldsymbol{\eta}^{n+1}; \boldsymbol{v}, \boldsymbol{\psi})^* + B(p^{n+1}; \boldsymbol{v}, \boldsymbol{\psi})^* = F_f^*(\boldsymbol{v}) + \widehat{F}_s\left(\frac{\boldsymbol{\psi}}{\Delta t}\right) \\
B(q; \boldsymbol{u}^{n+1}, \boldsymbol{\eta}^{n+1})^* = 0
\end{cases}
\tag{2}
$$

   for all $(\boldsymbol{v}, \widehat{\boldsymbol{\psi}}) \in \boldsymbol{Z}^*$ and $q \in Q^*$.
3. Update the fluid domain obtaining Ω_f^{n+1}.

The functionals F_f^* and F_s account for forcing terms, boundary data and terms coming from the time discretization. We point out that, thanks to the coupling condition $(1)_5$ and the particular choice of the fluid-structure test functions in $\boldsymbol{Z}^*$, the two interface terms coming from the integration by parts, namely $\int_{\Sigma^*} \boldsymbol{T}_f^{n+1} \boldsymbol{n} \cdot \boldsymbol{v} \, d\gamma$ and $\int_{\Sigma^*} \boldsymbol{T}_s^{n+1} \boldsymbol{n} \cdot \frac{\boldsymbol{\psi}}{\Delta t} \, d\gamma$, cancel out.

A second possibility is to treat the fluid domain and the convective term implicitly and to embed the fluid-structure problem into a fixed-point loop over the position of the FS interface Σ^*. However, for the sake of exposition we limit our attention to the semi-implicit case, discussing whenever appropriate the feasibility of the proposed approaches to implicit algorithms.

2.3   Weak formulation of the continuity velocity

In view of the numerical treatment of the flow rate problem based on the control theory introduced in Sect. 5, we introduce here a different formulation when the interface continuity conditions on the velocity are forced weakly. In this way, test functions on the fluid problem do not necessary match at the FS interface with the structures ones. Let $\boldsymbol{D}^*$ be the space $\boldsymbol{H}^{-1/2}(\Sigma^*)$. At time step t^{n+1}, we consider the following "augmented" variational formulation of the semi-discretized problem.

Given $\boldsymbol{f}_f^{n+1} \in L^2(\Omega_f^*)$ and $\widehat{\boldsymbol{f}}_s^{n+1} \in \boldsymbol{L}^2(\Omega_s^0)$, find $\boldsymbol{u}^{n+1} \in \boldsymbol{V}^*$, $p^{n+1} \in Q^*$, $\widehat{\boldsymbol{\eta}}^{n+1} \in \boldsymbol{W}$ and $\boldsymbol{\beta}^{n+1} \in \boldsymbol{D}^*$ such that,

$$
\begin{cases}
A(\boldsymbol{u}^{n+1}, \boldsymbol{\eta}^{n+1}; \boldsymbol{v}, \boldsymbol{\psi})^* + B(p^{n+1}; \boldsymbol{v}, \boldsymbol{\psi})^* + C(\boldsymbol{\beta}^{n+1}; \boldsymbol{v}, \boldsymbol{\psi})^* = F_f^*(\boldsymbol{v}) + \widehat{F}_s\left(\frac{\boldsymbol{\psi}}{\Delta t}\right) \\
B(q; \boldsymbol{u}^{n+1}, \boldsymbol{\eta}^{n+1})^* = 0 \\
C(\boldsymbol{\alpha}; \boldsymbol{u}^{n+1}, \boldsymbol{\eta}^{n+1})^* = \int_{\Sigma^*} \boldsymbol{\alpha} \cdot \frac{\boldsymbol{\eta}^n}{\Delta t} d\gamma
\end{cases}
$$

$$\tag{3}$$

for all $\boldsymbol{v} \in \boldsymbol{V}^*$, $q \in Q^*$, $\widehat{\boldsymbol{\psi}} \in \boldsymbol{W}$ and $\boldsymbol{\alpha} \in \boldsymbol{D}^*$ and where

$$C(\boldsymbol{\alpha}; \boldsymbol{v}, \boldsymbol{\psi})^* := - \int_{\Sigma^*} \boldsymbol{\alpha} \cdot \left(\boldsymbol{v} - \frac{\boldsymbol{\psi}}{\Delta t} \right) d\gamma.$$

From now on, we drop the index $^{n+1}$ for the sake of simplicity. Moreover, let us introduce the following norms

$$\|\boldsymbol{v}\|_{V^*} := \left(\|\boldsymbol{v}\|_f^2 + \|\nabla \boldsymbol{v}\|_f^2 \right)^{1/2},$$
$$\|\boldsymbol{\psi}\|_W := \left(\|\boldsymbol{\psi}\|_s^2 + \|\nabla \boldsymbol{\psi}\|_s^2 \right)^{1/2},$$

being $\| \cdot \|_f$ and $\| \cdot \|_s$ the $L^2(\Omega_f^*)$ and $L^2(\Omega_s^0)-$ norms. We have the following

Proposition 1 *If μ is big enough, problem (2) admits a unique solution $[\bar{\boldsymbol{u}}, \bar{p}, \bar{\boldsymbol{\eta}}]$. Problem (3) admits a unique solution too, namely $[\bar{\boldsymbol{u}}, \bar{p}, \bar{\boldsymbol{\eta}}, \boldsymbol{\beta}]$, with $\boldsymbol{\beta} = \bar{\boldsymbol{T}}_f \boldsymbol{n}|_{\Sigma^*} := \boldsymbol{T}_f(\bar{\boldsymbol{u}}, \bar{p}) \boldsymbol{n}|_{\Sigma^*}$.*

Proof. Let us introduce the following norm

$$\| (\boldsymbol{v}, \boldsymbol{\psi}) \|^2 := \|\boldsymbol{v}\|_{V^*}^2 + \left\| \frac{\widehat{\boldsymbol{\psi}}}{\Delta t} \right\|_W^2.$$

From the Korn's inequality, there exist two constants K_f and K_s such that (see, e.g, [5])

$$(\nabla \boldsymbol{v} + (\nabla \boldsymbol{v})^T, \boldsymbol{v})^* \geq K_f \|\boldsymbol{v}\|_{V^*},$$
$$(\widehat{\boldsymbol{T}}_s(\widehat{\boldsymbol{\psi}}), \tfrac{1}{\Delta t} \nabla \widehat{\boldsymbol{\psi}}) \geq \tfrac{K_s}{\Delta t} \|\widehat{\boldsymbol{\psi}}\|_W.$$

Then, if the viscosity μ is big enough, we have

$$A(\boldsymbol{v}, \boldsymbol{\psi}; \boldsymbol{v}, \boldsymbol{\psi}) \geq \frac{\rho_f}{\Delta t} \|\boldsymbol{v}\|_f^2 + \mu K_f \|\nabla \boldsymbol{v}\|_f^2 +$$

$$+ \rho_f (((\boldsymbol{v}^* - \boldsymbol{w}^*) \cdot \nabla) \boldsymbol{v}, \boldsymbol{v})_f^* + \rho_s \frac{1}{\Delta t^3} \|\boldsymbol{\psi}\|_s^2 + \frac{K_s}{\Delta t} \|\widehat{\boldsymbol{\psi}}\|_W \geq \gamma \| (\boldsymbol{v}, \boldsymbol{\psi}) \|^2,$$

where $\gamma = \min\{\rho_f/\Delta t, \mu K_f, K_s/\Delta t\}$. From classical arguments (see, e.g., [7,6]), the fluid problem is well-posed, then $\forall q \in Q^*$ there exists $\widetilde{\boldsymbol{v}} \in \boldsymbol{V}^*$ such that

$$-(q, \nabla \cdot \widetilde{\boldsymbol{v}}) \geq \sigma \|q\|_f \|\widetilde{\boldsymbol{v}}\|_{V^*},$$

for a suitable $\sigma > 0$. By choosing $\widetilde{\boldsymbol{\psi}} = \boldsymbol{0}$ we obtain

$$B(q; \widetilde{\boldsymbol{v}}, \widetilde{\boldsymbol{\psi}}) \geq \sigma \|q\|_f \|(\widetilde{\boldsymbol{v}}, \widetilde{\boldsymbol{\psi}})\|$$

$\forall q \in Q^*$, so that the fluid-structure problem (2) is proved to be well-posed as well.

Let us now show that the bilinear form C satisfies an *inf-sup* condition and therefore that problem (3) admits a unique solution (see [7]). More precisely, we will show that $\forall \boldsymbol{\alpha} \in \boldsymbol{D}^*$, there exists a couple $(\widetilde{\boldsymbol{v}}, \widetilde{\boldsymbol{\psi}}) \in \boldsymbol{Z}^*$ such that

$$C(\boldsymbol{\alpha}; \widetilde{\boldsymbol{v}}, \widetilde{\boldsymbol{\psi}})^* \geq \sigma_2 \|\boldsymbol{\alpha}\|_D \|(\widetilde{\boldsymbol{v}}, \widetilde{\boldsymbol{\psi}})\|, \tag{4}$$

for a suitable $\sigma_2 > 0$, where

$$\|\boldsymbol{\alpha}\|_D := \|\boldsymbol{\alpha}\|_{H^{-1/2}(\Sigma^*)} = \sup_{\|\boldsymbol{w}\|_{1/2}=1} \int_{\Sigma^*} \boldsymbol{\alpha} \cdot \boldsymbol{w} \, d\gamma$$

and

$$\|\boldsymbol{w}\|_{1/2} := \|\boldsymbol{w}\|_{H^{1/2}(\Sigma^*)} = \inf_{\substack{\boldsymbol{z} \in \boldsymbol{V}^* \\ \boldsymbol{z}|_{\Sigma^*}=\boldsymbol{w}}} \|\boldsymbol{z}\|_V.$$

Given $\boldsymbol{\alpha} \in \boldsymbol{D}^*$, let us choose $\widetilde{\boldsymbol{\psi}} \in \boldsymbol{W}$ such that $\left\|\dfrac{\widetilde{\boldsymbol{\psi}}}{\Delta t}\right\|_{1/2} = 1$ and such that

$\int_{\Sigma^*} \boldsymbol{\alpha} \cdot \dfrac{\widetilde{\boldsymbol{\psi}}}{\Delta t} d\gamma \geq \frac{1}{2}\|\boldsymbol{\alpha}\|_D$. We point out that this choice is always possible thanks to the definition of $\|\cdot\|_D$. Moreover, we choose $\widetilde{\boldsymbol{v}} \in \boldsymbol{V}^*$ such that $\|\widetilde{\boldsymbol{v}}\|_{1/2} = 1/4$. We obtain

$$C(\boldsymbol{\alpha}; \widetilde{\boldsymbol{v}}, \widetilde{\boldsymbol{\psi}})^* = -\int_{\Sigma^*} \boldsymbol{\alpha} \cdot \widetilde{\boldsymbol{v}} \, d\gamma + \int_{\Sigma^*} \boldsymbol{\alpha} \cdot \frac{\widetilde{\boldsymbol{\psi}}}{\Delta t} \, d\gamma \geq -\|\boldsymbol{\alpha}\|_D \|\widetilde{\boldsymbol{v}}\|_{1/2} + \frac{1}{2}\|\boldsymbol{\alpha}\|_D = \frac{1}{4}\|\boldsymbol{\alpha}\|_D.$$

Since $\|(\widetilde{\boldsymbol{v}}, \widetilde{\boldsymbol{\psi}})\| = \sqrt{1 + 1/16}$, we obtain

$$C(\boldsymbol{\alpha}; \widetilde{\boldsymbol{v}}, \widetilde{\boldsymbol{\psi}})^* \geq \frac{1}{4}\sqrt{\frac{16}{17}}\|\boldsymbol{\alpha}\|_D \|(\widetilde{\boldsymbol{v}}, \widetilde{\boldsymbol{\psi}})\|,$$

and therefore condition (4) is satisfied with $\sigma_2 = \frac{1}{\sqrt{17}}$.

It is now easy to show that the solutions of problem (2) and (3) coincide and that $\boldsymbol{\beta} = \bar{\boldsymbol{T}}_f \boldsymbol{n}|_{\Sigma^*}$ (see [1]). Let $[\bar{\boldsymbol{u}}, \bar{p}, \bar{\boldsymbol{\eta}}]$ be the solution of problem (2). We have for all $\boldsymbol{v} \in \boldsymbol{V}^*$, $q \in Q^*$, $\widehat{\boldsymbol{\psi}} \in \boldsymbol{W}$:

$$A(\bar{\boldsymbol{u}}, \bar{\boldsymbol{\eta}}; \boldsymbol{v}, \boldsymbol{\psi})^* + B(\bar{p}; \boldsymbol{v}, \boldsymbol{\psi}) = \int_{\Sigma^*} \bar{\boldsymbol{T}}_f \boldsymbol{n} \cdot \boldsymbol{v} \, d\gamma - \int_{\Sigma^*} \bar{\boldsymbol{T}}_s \boldsymbol{n} \cdot \frac{\boldsymbol{\psi}}{\Delta t} \, d\gamma + F_f^*(\boldsymbol{v}) + \widehat{F}_s\left(\frac{\boldsymbol{\psi}}{\Delta t}\right),$$

where the two terms at the FS interface come from the integration by parts of the fluid and structure equations in strong form. Then, by noticing that $C(\bar{\boldsymbol{T}}_f \boldsymbol{n}; \boldsymbol{v}, \boldsymbol{\psi})^* + \int_{\Sigma^*} \bar{\boldsymbol{T}}_f \boldsymbol{n} \cdot \left(\boldsymbol{v} - \frac{\boldsymbol{\psi}}{\Delta t}\right) d\gamma = 0$, we obtain

$$A(\bar{\boldsymbol{u}}, \bar{\boldsymbol{\eta}}; \boldsymbol{v}, \boldsymbol{\psi})^* + B(\bar{p}; \boldsymbol{v}, \boldsymbol{\psi}) + C(\bar{\boldsymbol{T}}_f \boldsymbol{n}; \boldsymbol{v}, \boldsymbol{\psi})^* = \int_{\Sigma^*} \bar{\boldsymbol{T}}_f \boldsymbol{n} \cdot \boldsymbol{v} \, d\gamma - \int_{\Sigma^*} \bar{\boldsymbol{T}}_s \boldsymbol{n} \cdot \frac{\boldsymbol{\psi}}{\Delta t} \, d\gamma +$$

$$+ F_f^*(\boldsymbol{v}) + \widehat{F}_s\left(\frac{\boldsymbol{\psi}}{\Delta t}\right) - \int_{\Sigma^*} \bar{\boldsymbol{T}}_f \boldsymbol{n} \cdot \left(\boldsymbol{v} - \frac{\boldsymbol{\psi}}{\Delta t}\right) d\gamma.$$

9

Finally, owing to $(1)_5$, we obtain

$$A(\bar{\boldsymbol{u}}, \bar{\boldsymbol{\eta}}; \boldsymbol{v}, \boldsymbol{\psi})^* + B(\bar{p}; \boldsymbol{v}, \boldsymbol{\psi}) + C(\bar{\boldsymbol{T}}_f \boldsymbol{n}; \boldsymbol{v}, \boldsymbol{\psi})^* = F_f^*(\boldsymbol{v}) + \widehat{F}_s\left(\frac{\boldsymbol{\psi}}{\Delta t}\right),$$

that is $(3)_1$ is satisfied with $\boldsymbol{\beta} = \bar{\boldsymbol{T}}_f \boldsymbol{n}|_{\Sigma^*}$. Moreover, from $(1)_4$ we have

$$B(\boldsymbol{\alpha}; \bar{\boldsymbol{u}}, \bar{\boldsymbol{\eta}})^* = -\int_{\Sigma^*} \boldsymbol{\alpha} \cdot \left(\bar{\boldsymbol{u}} - \frac{\bar{\boldsymbol{\eta}}}{\Delta t}\right) d\gamma = -\int_{\Sigma^*} \boldsymbol{\alpha} \cdot \frac{\bar{\boldsymbol{\eta}}^n}{\Delta t} d\gamma$$

and then also $(3)_2$ is fulfilled. Therefore, the Lagrange multiplier $\boldsymbol{\beta}$ has the physical meaning of normal stress at the FS interface.

On the other hand, if $[\bar{\boldsymbol{u}}, \bar{p}, \bar{\boldsymbol{\eta}}, \bar{\boldsymbol{\beta}}]$ is solution of (3), then by exploiting the property of the test functions in $\boldsymbol{Z}^*$, it follows that $[\bar{\boldsymbol{u}}, \bar{p}, \bar{\boldsymbol{\eta}}]$ is solution of (2). □

In the next three Sections we introduce three different formulations of the Flow rate/FSI problem. For this reason, from now on we set $\Gamma_F^t \neq \emptyset$.

3 Partitioned methods for the Flow-rate/FSI problems

An immediate class of methods for the Flow-rate/FSI problems stems by the staggered or partitioned approaches for solving fluid-structure interaction (see e.g. [11], Chap. 9). When fluid and structure are solved separately, at each step we resort to a rigid fluid problem in a "frozen" domain. Numerical methods for the flow rate problems in rigid domains can be therefore applied at each iterative step.

Let us consider the time discretization of system (1), where a flow rate condition is prescribed on the artificial sections Γ_j^*, namely

$$\int_{\Gamma_j^*} \boldsymbol{u}^{n+1} \cdot \boldsymbol{n} \, d\gamma = F_j^{n+1}, \qquad j = 1, \ldots, m, \tag{5}$$

where $F_j^{n+1} = F_j(t^{n+1})$ are given functions of time. We point out the semi-implicit treatment of the interface position.

For the sake of generality, we refer to the class of partitioned procedures introduced in [3] as *Robin-Robin* schemes. For the ease of notation let us drop the index $^{n+1}$ of the current time step. We have the following

Algorithm 1

Given two parameters $\alpha_f \neq \alpha_s$, the quantities at the previous time step, $\boldsymbol{\eta}^n$, $\boldsymbol{\eta}^{n-1}$ and $\boldsymbol{u}^n$, and the value of the structure displacement at the current iteration $\boldsymbol{\eta}^k$, find the value of the solution at the next iteration $\boldsymbol{\eta}^{k+1}$, $\boldsymbol{u}^{k+1}$ and p^{k+1} by solving the following steps

1. Flow rate/fluid problem (Robin boundary condition)

$$
\begin{cases}
\rho_f \frac{\boldsymbol{u}^{k+1}-\boldsymbol{u}^n}{\Delta t} + \rho_f(\boldsymbol{u}^* - \boldsymbol{w}^*) \cdot \nabla \boldsymbol{u}^{k+1} - \nabla \cdot \boldsymbol{T}_f^{k+1} = \boldsymbol{f}_f & \text{in } \Omega_f^*, \\
\nabla \cdot \boldsymbol{u}^{k+1} = 0 & \text{in } \Omega_f^*, \\
\int_{\Gamma_j^*} \rho_f \boldsymbol{u}^{n+1} \cdot \boldsymbol{n}\, d\gamma = F_j^{n+1}, \quad j = 1, \dots, m \\
\alpha_f \boldsymbol{u}^{k+1} + \boldsymbol{T}_f^{k+1}\boldsymbol{n} = \alpha_f \frac{\boldsymbol{\eta}^k - \boldsymbol{\eta}^n}{\Delta t} + \boldsymbol{T}_s^k \boldsymbol{n} & \text{on } \Sigma^*.
\end{cases}
\tag{6}
$$

2. Structure problem (Robin boundary condition)

$$
\begin{cases}
\rho_s \frac{\widehat{\boldsymbol{\eta}}^{k+1} - 2\widehat{\boldsymbol{\eta}}^n + \widehat{\boldsymbol{\eta}}^{n-1}}{\Delta t^2} - \nabla \cdot \widehat{\boldsymbol{T}}_s^{k+1} = \widehat{\boldsymbol{f}}_s & \text{in } \Omega_0^s, \\
\frac{\alpha_s}{\Delta t}\boldsymbol{\eta}^{k+1} + \boldsymbol{T}_s^{k+1}\boldsymbol{n} = \frac{\alpha_s}{\Delta t}\boldsymbol{\eta}^n + \alpha_s \boldsymbol{u}^{k+1} + \boldsymbol{T}_f^{k+1}\boldsymbol{n} & \text{on } \Sigma^*.
\end{cases}
$$

For a description of optimal choices of parameters α_f and α_s, we refer the reader to [3]. The previous algorithm defines a class of schemes. For example, if $\alpha_f \to \infty$ and $\alpha_s = 0$ we recover the well-known *Dirichlet-Neumann* (DN) scheme. In [3] it has been shown that among all the possible schemes of this class, the *Robin-Neumann (RN)* ($\alpha_s = 0$) is the one with the best convergence properties. For this reason, we consider this scheme in the numerical simulations reported in Sect. 6.

Algorithm 1 splits the solution of the fluid and the structure problems in an iterative framework and contains a flow rate problem at each iteration. The latter can be solved by considering one of the strategies proposed for the solution of a flow-rate problem in the rigid case (see [14,10,18,19,12]). Indeed, at each time step, the fluid problem (6) is solved in a fixed domain Ω_f^*.

Remark 1 *Due to the mass conservation, in the rigid case it is not possible to prescribe an arbitrary flow rate on all the artificial sections Γ_i^t, $i = 1, \dots, m$, if $\Gamma_N^t = \emptyset$. In the compliant case this compatibility condition does not hold anymore. Nevertheless, as pointed out in [16,2], if we use a partitioned procedure in which the structure prescribes a Dirichlet condition at the interface to the fluid (as, e.g., in the Dirichlet-Neumann algorithm) an incompatibility might arise between the flow rates F_i, $i = 1, \dots, m,$, the velocity on Γ_D^t and*

the velocity at the interface, and then the mass conservation

$$\int_{\Sigma^t} \frac{\partial \boldsymbol{\eta}}{\partial t} \cdot \boldsymbol{n} \, d\gamma = \int_{\Gamma_D^t} \boldsymbol{u} \cdot \boldsymbol{n} \, d\gamma + \sum_{i=1}^{m} F_i(t) \tag{7}$$

is not in general satisfied. However, when adopting Robin-Robin schemes, on Σ^t we prescribe a Robin condition in place of a Dirichlet one, so that mass conservation (7) is still fulfilled, for all the choices of F_i, $i = 1, \ldots, m$ and of the Dirichlet datum on Γ_D^t.

We point out that the previous algorithm extends easily to the implicit treatment of the FS interface, simply by considering it in a fixed-point loop.

4 Augmented formulation of the Flow-rate/FSI problem

We extend here to the FSI case the augmented formulation proposed in [10] for the flow rate problem in the rigid case. In Sect. 4.1 we introduce the continuous formulation and in Sect. 4.2 we introduce the related algebraic problem. We also detail the *GMRes+Schur complement (GSC)* scheme for its numerical solution.

4.1 The augmented variational formualation

Let us consider the flow rate conditions (5) as constraints to be forced to the variational formulation of the FSI problem (2), by the introduction of a Lagrange multiplier λ_j, one for each flow-rate condition. Here we force the continuity of the velocity in an essential way. Then the augmented formulation for the flow-rate/FSI problem reads:

Given $\boldsymbol{f}_f^{n+1} \in L^2(\Omega_f^*)$ and $\widehat{\boldsymbol{f}}_s^{n+1} \in \boldsymbol{L}^2(\Omega_s^0)$, find $(\boldsymbol{u}^{n+1}, \widehat{\boldsymbol{\eta}}^{n+1}) \in \boldsymbol{Z}^*$, $p^{n+1} \in Q^*$ and $\boldsymbol{\lambda}^{n+1} \in \mathbb{R}$ such that,

$$\begin{cases} A(\boldsymbol{u}^{n+1}, \boldsymbol{\eta}^{n+1}; \boldsymbol{v}, \boldsymbol{\psi})^* + B(p^{n+1}; \boldsymbol{v}, \boldsymbol{\psi})^* + D(\boldsymbol{\lambda}^{n+1}; \boldsymbol{v}, \boldsymbol{\psi})^* = F_f^*(\boldsymbol{v}) + \widehat{F}_s\left(\frac{\boldsymbol{\psi}}{\Delta t}\right) \\ B(q; \boldsymbol{u}^{n+1}, \boldsymbol{\eta}^{n+1})^* = 0 \\ D(\boldsymbol{\nu}; \boldsymbol{u}^{n+1}, \boldsymbol{\eta}^{n+1})^* = \sum_{i=1}^{m} \nu_i F_i^{n+1} \end{cases} \tag{8}$$

for all $(\boldsymbol{v}, \boldsymbol{\psi}) \in \boldsymbol{Z}^*$, $q \in Q^*$ and $\boldsymbol{\nu} \in \mathbb{R}^m$ and where

$$D(\boldsymbol{\nu}; \boldsymbol{v}, \boldsymbol{\psi})^* := \sum_{j=1}^{m} \nu_j \int_{\Gamma_j^*} \boldsymbol{v} \cdot \boldsymbol{n} \, d\gamma.$$

Remark 2 *As proven in [18], the bilinear form $D(\cdot; \cdot, \cdot)$ satisfies an inf-sup condition. Therefore, the augmented/FSI problem well-posedness is inherited by well-posedness results of the non augmented FSI problem.*

4.2   The algebraic problem and the GSC algorithm

We discretize in time with the schemes illustrated in Sect. 2 and in space with Lagrangian finite elements. To this aim, we introduce a triangulation of fluid and structure domains and we assume that the meshes are conformal at the interface Σ^*. At each time step t^{n+1}, we obtain the following linear system

$$\begin{bmatrix} A^* & (\widetilde{\Phi}^*)^T \\ \widetilde{\Phi}^* & 0 \end{bmatrix} \begin{bmatrix} \boldsymbol{X}^{n+1} \\ \boldsymbol{\Lambda}^{n+1} \end{bmatrix} = \begin{bmatrix} \boldsymbol{b}^{n+1} \\ \boldsymbol{F}^{n+1}, \end{bmatrix}. \tag{9}$$

where

$$A^* = \begin{bmatrix} C^*_{ff} & G^*_f & C^*_{f\Sigma} & 0 & 0 \\ D^*_f & 0 & D^*_\Sigma & 0 & 0 \\ 0 & 0 & M^*_\Sigma & -M_\Sigma/\Delta t & 0 \\ C^*_{\Sigma f} & G^*_\Sigma & C^*_{\Sigma\Sigma} & S_{\Sigma\Sigma} & S_{\Sigma s} \\ 0 & 0 & 0 & S_{s\Sigma} & S_{ss} \end{bmatrix}, \quad \boldsymbol{X}^{n+1} = \begin{bmatrix} \boldsymbol{U}^{n+1}_f \\ \boldsymbol{P}^{n+1} \\ \boldsymbol{U}^{n+1}_\Sigma \\ \boldsymbol{D}^{n+1}_\Sigma \\ \boldsymbol{D}^{n+1}_s \end{bmatrix},$$

$$\boldsymbol{b}^{n+1} = \begin{bmatrix} \mathbf{b}^{n+1}_f \\ \mathbf{0} \\ -M_\Sigma/\Delta t\, \boldsymbol{D}^n_\Sigma \\ \mathbf{b}^{n+1}_\Sigma \\ \mathbf{b}^{n+1}_s \end{bmatrix}, \quad \widetilde{\Phi}^{n+1} = \begin{bmatrix} \Phi^{n+1} & 0 \end{bmatrix}.$$

We have set $\Phi^*_{ij} = \int_{\Gamma^*_i} \boldsymbol{l}_j \cdot \boldsymbol{n}\, d\gamma$, where the $\boldsymbol{l}_i$'s are the Lagrange basis functions related to the fluid velocity. M_Σ is the mass matrix at the interface Σ^* and the size of the zero-matrices is understood. Moreover $\mathbf{U}^{n+1}_f$ is the vector of nodal values of the fluid velocity at the interior nodes, $\mathbf{U}^{n+1}_\Sigma$ that at the FS interface, $\mathbf{P}^{n+1}$ is the vector of (interior and interface) nodal values for the pressure. $\mathbf{D}^{n+1}_s$ and $\mathbf{D}^{n+1}_\Sigma$ contain the structure degrees of freedom related to interior and interface nodes, respectively. Finally, $\boldsymbol{\Lambda}^{n+1}$ is the vector of Lagrange multipliers. The right hand side $\mathbf{b}^{n+1}$ accounts for external forces, boundary data and other terms related to the time discretization scheme, whilst $\boldsymbol{F}^{n+1}$ is the vector whose component are the data F^{n+1}_j. The first two

rows of (9) are the fully discrete versions of the flow-rate/momentum and mass conservation equations for the fluid. The third equation states the continuity of velocities on the interface and is the algebraic counterpart of $(1)_4$. The fourth row enforces continuity of the normal stresses at the interface in weak form and the fifth row is the structure problem for the internal nodes. Finally, the last row is the algebraic counterpart of the flow-rate conditions (5).

Following [10,18], we can formally eliminate the unknown $\boldsymbol{X}^{n+1}$ from the first equation of system (9). Dropping for the sake of simplicity the index $^{n+1}$, we obtain an equation for the unknown $\boldsymbol{\Lambda}$ solely, namely

$$\widetilde{\Phi}(A^*)^{-1}\widetilde{\Phi}^T\boldsymbol{\Lambda} = \widetilde{\Phi}(A^*)^{-1}\boldsymbol{b} - \boldsymbol{F}, \qquad (10)$$

which is a linear system of dimension m. We point out that with $(A^*)^{-1}$ we indicate formally the solution of a FSI problem with Neumann conditions at the artificial sections.

Since the bilinear form $D(\cdot;\cdot,\cdot)$ satisfies an inf-sup condition, it follows that $ker(\widetilde{\Phi})^T = \emptyset$. Then, if the algebraic-FSI problem admits a unique solution (that is if A^* is invertible), $\widetilde{\Phi}(A^*)^{-1}\widetilde{\Phi}^T$ is formally invertible and a unique solution $\boldsymbol{\Lambda}$ does exist. Therefore, we can formally apply an iterative methods, such as *GMRes*, to system (10) (as done in [18]). In particular, we have

Algorithm 2 *: GMRes + Schur Complement*

```
For each n solve:
```

$\quad\boldsymbol{\Lambda}_0 = (\lambda_{01}, \ldots, \lambda_{0m})$ is given
a) $A^*\boldsymbol{X}_1 = \boldsymbol{b} - (\widetilde{\Phi}^*)^T\boldsymbol{\Lambda}_0$
$\quad\boldsymbol{r}_0 = \widetilde{\Phi}^*\boldsymbol{X}_1 - \boldsymbol{F}$
$\quad\boldsymbol{v}_1 = \frac{\boldsymbol{r}_0}{\|\boldsymbol{r}_0\|}$
$\quad$for $j = 1, \ldots, m$
$\quad\quad\boldsymbol{\eta}_j = (\widetilde{\Phi}^*)^T\boldsymbol{v}_j$
b) $A^*\boldsymbol{Y}_j = \boldsymbol{\eta}_j$
$\quad\quad\boldsymbol{w}_j = \widetilde{\Phi}^*\boldsymbol{Y}_j$
$\quad\quad\quad$for $l = 1, \ldots, j$
$\quad\quad\quad h_{lj} = (\boldsymbol{w}_j, \boldsymbol{v}_l)$
$\quad\quad\quad\boldsymbol{w}_j = \boldsymbol{w}_j - h_{lj}\boldsymbol{v}_l$
$\quad\quad\quad$end
$\quad\quad h_{j+1,j} = \|\boldsymbol{w}_j\|$
$\quad\quad$if $h_{j+1,j} = 0$
$\quad\quad n = j$ go to $(+)$
$\quad\quad$else $\boldsymbol{v}_{j+1} = \frac{\boldsymbol{w}_j}{h_{j+1,j}}$
$\quad\quad$end
$\quad$end
$\quad(+)\ \boldsymbol{z} = min\|\|\boldsymbol{r}_0\|\boldsymbol{e}_1 - H_n\boldsymbol{z}\|, \qquad H_m \in \mathbb{R}^{m+1} \times \mathbb{R}^m : H = [h_{ij}]$

$$\boldsymbol{\Lambda} = \boldsymbol{\Lambda}_0 + V\boldsymbol{z}, \qquad V = [\boldsymbol{v}_1 \, \ldots \, \boldsymbol{v}_m]$$
$$\boldsymbol{X} = \boldsymbol{X}_1 - Y\boldsymbol{z}, \qquad Y = [\boldsymbol{y}_1 \, \ldots \, \boldsymbol{y}_m] \quad \diamond$$

This algorithm is quite expensive, since at each time step it requires to solve $m+1$ FSI problems, indicated at points a) and b) in the algorithm. However, the algorithm allows to compute the unknown $\boldsymbol{X}$ at the last step without solving any additional linear system. Obviously, each of FSI problems can be solved with any of the strategies proposed in the literature (partitioned, monolithical, etc.), since all of them are equipped with standard Neumann boundary conditions at each of the artificial sections. Despite its cost, this algorithm is of practical use when one have at disposal a black-box FSI solver, without the possibility to treating the fluid and the structure subproblems separately.

We point out that the previous algorithm extends easily to the implicit case, simply by considering it in the fixed-point loop for the implicit treatement of the interface position.

5 Control theory-based approach

In this section we extend to the compliant flow rate problem the strategy introduced for the rigid case in [12]. In particular, we seek for constant in space Neumann data at the artificial sections which enforce in some sense the flow rate conditions. We limit our attention only to the semi-implicit treatment of the interface position. Indeed, the implicit treatment would require to consider also the shape derivatives, that is the derivatives of the fluid domain (which is unknown in this case) with respect to the other unknowns of the problem. This case will be considered in a forthcoming study.

5.1 Reformulation of the problem

Let us define the *state problem* by considering problem (3) equipped with Neumann boundary conditions at the artificial sections, given, at each t^{n+1}, by

$$\boldsymbol{T}_f \, \boldsymbol{n} = -k_j^{n+1} \boldsymbol{n}, \quad \text{on } \Gamma_j^*, \qquad j = 1, \ldots, m, \tag{11}$$

where the $k_j's$ are the *control variables* and we have set $k_j^{n+1} = k_j(t^{n+1})$. Therefore, the weak formulation of the state problem with a weak prescription

15

of the interface velocities (see Section 2.3) reads

$$
\begin{cases}
A(\boldsymbol{u}^{n+1}, \boldsymbol{\eta}^{n+1}; \boldsymbol{v}, \boldsymbol{\psi})^* + B(p^{n+1}; \boldsymbol{v}, \boldsymbol{\psi})^* + C(\boldsymbol{\beta}^{n+1}; \boldsymbol{v}, \boldsymbol{\psi})^* + \\
\qquad + \sum_{j=1}^m k_j^{n+1} \int_{\Gamma_j^*} \boldsymbol{v} \cdot \boldsymbol{n} \, d\gamma = F_f^*(\boldsymbol{v}) + \widehat{F}_s\left(\frac{\boldsymbol{\psi}}{\Delta t}\right) \\
B(q; \boldsymbol{u}^{n+1}, \boldsymbol{\eta}^{n+1})^* = 0 \\
C(\boldsymbol{\alpha}; \boldsymbol{u}^{n+1}, \boldsymbol{\eta}^{n+1})^* = \int_{\Sigma^*} \boldsymbol{\alpha} \cdot \frac{\boldsymbol{\eta}^n}{\Delta t} d\gamma
\end{cases}
\tag{12}
$$

for all $\boldsymbol{v} \in \boldsymbol{V}^*$, $q \in Q^*$, $\widehat{\boldsymbol{\psi}} \in \boldsymbol{W}$ and $\boldsymbol{\alpha} \in \boldsymbol{D}^*$.

We introduce at each time step t^l the following functional (see [12])

$$
J_F(\boldsymbol{z}) = \frac{1}{2} \sum_{j=1}^m \left(\int_{\Gamma_j^*} \boldsymbol{z} \cdot \boldsymbol{n} \, d\gamma - F_j^l \right)^2,
\tag{13}
$$

which is clearly minimal (and equal to zero) if conditions (5) are satisfied and $\boldsymbol{z} = \boldsymbol{u}^l$.

The Lagrangian functional related to (13) constrained with the state problem (12), given $\boldsymbol{u}^n$, $\boldsymbol{\eta}^n$ and $\boldsymbol{\eta}^{n-1}$, reads

$$
\mathcal{L}(\boldsymbol{U}, P, \boldsymbol{H}, \boldsymbol{B}; \boldsymbol{\lambda}_U, \lambda_P, \boldsymbol{\lambda}_H, \boldsymbol{\lambda}_B; \boldsymbol{K}) = J_F(\boldsymbol{U}) + A(\boldsymbol{U}, \boldsymbol{H}; \boldsymbol{\lambda}_U, \boldsymbol{\lambda}_H)^* + B(P; \boldsymbol{\lambda}_U, \boldsymbol{\lambda}_H)^* +
$$

$$
+ C(\boldsymbol{B}; \boldsymbol{\lambda}_U, \boldsymbol{\lambda}_H)^* + B(\lambda_p; \boldsymbol{U}, \boldsymbol{H})^* + C(\boldsymbol{\lambda}_B; \boldsymbol{U}, \boldsymbol{H})^* + \sum_{j=1}^m \int_{\Gamma_j^*} K_j \boldsymbol{\lambda}_u \cdot \boldsymbol{n} \, d\gamma +
$$

$$
- \int_{\Sigma^*} \boldsymbol{\lambda}_B \cdot \frac{\boldsymbol{\eta}^n}{\Delta t} d\gamma - F_f^*(\boldsymbol{\lambda}_U) - \widehat{F}_s\left(\frac{\widehat{\boldsymbol{\lambda}}_H}{\Delta t}\right).
\tag{14}
$$

Here, the quantities $\boldsymbol{\lambda}_U$, λ_P, $\boldsymbol{\lambda}_H$ and $\boldsymbol{\lambda}_B$ are the adjoint variables associated to the state variables $\boldsymbol{U}$, P, $\boldsymbol{H}$ and $\boldsymbol{B}$, respectively. From now on, for the sake of simplicity we drop the temporal index $^{n+1}$. In order to find the corresponding Euler equations, we impose that in correspondance of the solution $[\boldsymbol{u}, p, \boldsymbol{\eta}, \boldsymbol{\beta}; \boldsymbol{\lambda}_u, \lambda_p, \boldsymbol{\lambda}_\eta, \boldsymbol{\lambda}_\beta; \boldsymbol{k}]$ the Gateaux differentials of $\mathcal{L}$ evaluated for any test function vanish. Let us introduce the following notation. Given N Hilbert spaces $Z_1, \ldots, Z_N$, let $\boldsymbol{Z} = Z_1 \times Z_2 \times \ldots \times Z_N$ and $\mathcal{M} : \boldsymbol{Z} \to \mathbb{R}$, be such that $(y_1, \ldots, y_N) \in \boldsymbol{Z} \to \mathcal{M}(y_1, \ldots, y_N) \in \mathbb{R}$, and let $< \cdot, \cdot >$ be the duality pairing between Z' and $\boldsymbol{Z}$. We indicate with

$$
< d\mathcal{M}_{y_j}[z_1, \ldots, z_N], g > =
$$

$$
= \lim_{\varepsilon \to 0} \left(\frac{\mathcal{M}(y_1, \ldots, y_j + \varepsilon g, \ldots, y_N) - \mathcal{M}(y_1, \ldots, y_j, \ldots, y_N)}{\varepsilon} \right)\Bigg|_{\boldsymbol{y}=\boldsymbol{z}}
$$

the Gateaux differential of $\mathcal{M}$ with respect to y_j, computed at $\boldsymbol{z} = (z_1, \ldots, z_N) \in \boldsymbol{Z}$ and acting along the direction $g \in Z_j$. For the sake of notation, we will set $< d\mathcal{M}_{z_j}, g > = < d\mathcal{M}_{y_j}[z_1, \ldots, z_N], g >$.

Then, the solution which minimizes functional $J(\cdot)$ under the constraint is a stationary point of the Lagrangian functional and therefore can be computed by imposing that the gradient of $\mathcal{L}$ vanishes. In particular, by setting to zero the Gateaux derivatives of the Lagrangian functional with respect to the state variables we obtain the *adjoint problem*, namely

$$
\begin{cases}
< d\mathcal{L}_{\boldsymbol{u}}, \boldsymbol{v} > + < d\mathcal{L}_{\boldsymbol{\eta}}, \frac{\psi}{\Delta t} >= 0 \\
< d\mathcal{L}_{p}, q >= 0 \\
< d\mathcal{L}_{\boldsymbol{\beta}}, \boldsymbol{\alpha} >= 0,
\end{cases}
$$

for all $\boldsymbol{v} \in \boldsymbol{V}^{*}$, $q \in Q^{*}$, $\widehat{\psi} \in \boldsymbol{W}$ and $\boldsymbol{\alpha} \in \boldsymbol{D}^{*}$. *Optimality conditions* are obtained by vanishing derivatives with respect to the control variables

$$
< d\mathcal{L}_{k_{j}}, \nu >= 0, \quad j = 1, \ldots, m,
$$

for all $\nu \in \mathbb{R}$. These two problems together with the state problem

$$
\begin{cases}
< d\mathcal{L}_{\boldsymbol{\lambda}_{u}}, \boldsymbol{v} > + < d\mathcal{L}_{\boldsymbol{\lambda}_{\eta}}, \frac{\psi}{\Delta t} >= 0 \\
< d\mathcal{L}_{\lambda_{p}}, q >= 0 \\
< d\mathcal{L}_{\boldsymbol{\lambda}_{\beta}}, \boldsymbol{\alpha} >= 0,
\end{cases}
$$

for all $\boldsymbol{v} \in \boldsymbol{V}^{*}$, $q \in Q^{*}$, $\widehat{\psi} \in \boldsymbol{W}$ and $\boldsymbol{\alpha} \in \boldsymbol{D}^{*}$, yield the following coupled system.

Given $\boldsymbol{F} \in \mathbb{R}^{m}$, $\boldsymbol{f}_{f} \in \boldsymbol{L}^{2}(\Omega_{f}^{*})$ and $\boldsymbol{f}_{s} \in \boldsymbol{L}^{2}(\Omega_{s}^{0})$ find $\boldsymbol{k} \in \mathbb{R}^{m}$, $\boldsymbol{u} \in \boldsymbol{V}^{*}, p \in$

$Q^*, \boldsymbol{\eta} \in \boldsymbol{W}, \boldsymbol{\beta} \in \boldsymbol{D}^*, \lambda_u \in \boldsymbol{V}^*, \lambda_p \in Q^*, \boldsymbol{\lambda}_\eta \in \boldsymbol{W}$ and $\boldsymbol{\lambda}_\beta \in \boldsymbol{D}^*$, such that

State problem
$$
\begin{cases}
A(\boldsymbol{u}, \boldsymbol{\eta}; \boldsymbol{v}, \boldsymbol{\psi})^* + B(p; \boldsymbol{v}, \boldsymbol{\psi})^* + C(\boldsymbol{\beta}; \boldsymbol{v}, \boldsymbol{\psi})^* + \\
\quad + \sum_{j=1}^m k_j \int_{\Gamma_j^*} \boldsymbol{v} \cdot \boldsymbol{n}\, d\gamma = F_f^*(\boldsymbol{v}) + \widehat{F}_s\left(\frac{\boldsymbol{\psi}}{\Delta t}\right) \\
B(q; \boldsymbol{u}, \boldsymbol{\eta})^* = 0 \\
C(\boldsymbol{\alpha}; \boldsymbol{u}, \boldsymbol{\eta})^* = \int_{\Sigma^*} \boldsymbol{\alpha} \cdot \frac{\boldsymbol{\eta}^n}{\Delta t} d\gamma
\end{cases}
$$

$$(15a)$$

Adjoint problem
$$
\begin{cases}
A(\boldsymbol{v}, \boldsymbol{\psi}; \boldsymbol{\lambda}_u, \boldsymbol{\lambda}_\eta)^* + B(\lambda_p; \boldsymbol{v}, \boldsymbol{\psi})^* + C(\boldsymbol{\lambda}_\beta; \boldsymbol{v}, \boldsymbol{\psi})^* + \\
\quad + \sum_{j=1}^m \left(\int_{\Gamma_j^*} \boldsymbol{u} \cdot \boldsymbol{n}\, d\gamma - F_j\right) \int_{\Gamma_j^*} \boldsymbol{v} \cdot \boldsymbol{n}\, d\gamma = 0 \\
B(q; \boldsymbol{\lambda}_u, \boldsymbol{\lambda}_\eta)^* = 0 \\
C(\boldsymbol{\alpha}; \boldsymbol{\lambda}_u, \boldsymbol{\lambda}_\eta)^* = 0
\end{cases}
$$

$$(15b)$$

Optimality conditions $\displaystyle\int_{\Gamma_j^*} \nu \boldsymbol{\lambda}_u \cdot \boldsymbol{n}\, d\gamma = 0, \quad j = 1, \dots, m$ (15c)

for all $\boldsymbol{v} \in \boldsymbol{V}^*$, $q \in Q^*$, $\boldsymbol{\psi} \in \boldsymbol{W}$, $\boldsymbol{\alpha} \in \boldsymbol{D}^*$ and $\nu \in \mathbb{R}$.

We point out that system (15) couples two linearized fluid-structure inter-action problems and m scalar equations. For its numerical solution, we can resort to iterative techniques. As already done for the rigid case (see [12]), it is worth noting that, if the iterative process converges, at the limit, i.e. when $J_F = 0$, the fulfillment of the adjoint problem and of the optimality conditions implies that the adjoint solution is equal to zero. Indeed, the adjoint problem is linear with the only forcing term given by the Neumann boundary condi-tions at the artificial sections Γ_j^* which, clearly, are zero when $J_F = 0$. The adjoint variables are however needed to drive iterative schemes to the optimal solution.

Weak imposition of the continuity of the velocity at the interface has been preferred since the interface condition for the adjoint problem in this way are easily derived. In particular, it is given by

$$
\frac{\boldsymbol{\lambda}_\eta}{\Delta t} = \boldsymbol{\lambda}_u \quad \text{on} \quad \Sigma^*.
$$

The next result states the well-posedness of system (15).

Proposition 2 *If problem (2) admits a unique solution, then also system (15) admits a unique solution.*

Proof. The proof follows the same guidelines of Proposition 2.1 in [12]. For

18

any $\boldsymbol{h} = [h_1, \ldots, h_m]$, let $\mathcal{P}_{S_1,S_2}(\boldsymbol{h})$ be the velocity $\boldsymbol{u}$ solution of problem

$$
\begin{cases}
A(\boldsymbol{u}, \boldsymbol{\eta}; \boldsymbol{v}, \boldsymbol{\psi})^* + B(p; \boldsymbol{v}, \boldsymbol{\psi})^* + C(\boldsymbol{\beta}; \boldsymbol{v}, \boldsymbol{\psi})^* = -\sum_{j=1}^m h_j \int_{\Gamma_j^*} \boldsymbol{v} \cdot \boldsymbol{n} \, d\gamma + S_1(\boldsymbol{v}, \boldsymbol{\psi}) \\
B(q; \boldsymbol{u}, \boldsymbol{\eta})^* = 0 \\
C(\boldsymbol{\alpha}; \boldsymbol{u}, \boldsymbol{\eta})^* = S_2(\boldsymbol{\alpha}),
\end{cases}
$$

$$(16)$$

$\forall \boldsymbol{v} \in \boldsymbol{V}^*$, $q \in Q^*$, $\boldsymbol{\psi} \in \boldsymbol{W}$ and $\boldsymbol{\alpha} \in \boldsymbol{D}^*$, where $S_1(\boldsymbol{v}, \boldsymbol{\psi})$ and $S_2(\boldsymbol{\alpha})$ are a given form and functional, respectively. Moreover, let $\mathcal{A}\boldsymbol{v}$ be the vector whose $j-th$ component is $\int_{\Gamma_j} \boldsymbol{v} \cdot \boldsymbol{n} \, d\gamma$, and $\mathcal{B}_{S_1,S_2} := \mathcal{A}\mathcal{P}_{S_1,S_2}$. Then, by setting

$$
G_1(\boldsymbol{v}, \boldsymbol{\psi}) := F_f^*(\boldsymbol{v}) + \widehat{F}_s\left(\frac{\widehat{\boldsymbol{\psi}}}{\Delta t}\right)
$$

$$
G_2(\boldsymbol{\alpha}) := \int_{\Sigma^*} \boldsymbol{\alpha} \cdot \frac{\boldsymbol{\eta}^n}{\Delta t} d\gamma,
$$

we can write system (15) in term of the only unknown $\boldsymbol{k}$, as

$$
\mathcal{B}_{0,0}[\mathcal{B}_{G_1,G_2}(\boldsymbol{k}) - \boldsymbol{F}] = \boldsymbol{0}. \tag{17}
$$

Moreover, by setting $[\boldsymbol{u}_i, p_i, \boldsymbol{\eta}_i, \boldsymbol{\beta}_i]$ as the solution of (16) with $S_1 = S_2 = 0$ and $\boldsymbol{h} = \boldsymbol{e}_j$, being $\boldsymbol{e}_j$ the $j-th$ unit vector, from (16) we have, by choosing $[\boldsymbol{u}_j, p_j, \boldsymbol{\eta}_j, \boldsymbol{\beta}_j]$ as test functions and by setting $\boldsymbol{h} = \boldsymbol{e}_i$, $S_1 = 0$ and $S_2 = 0$,

$$
A(\boldsymbol{u}_i, \boldsymbol{\eta}_i; \boldsymbol{u}_j, \boldsymbol{\eta}_j)^* = -\int_{\Gamma_i^*} \boldsymbol{u}_j \cdot \boldsymbol{n} \, d\gamma.
$$

This implies that matrix $\mathcal{B}_{0,0}$ has component

$$
[\mathcal{B}_{0,0}]_{ij} = -A(\boldsymbol{u}_i, \boldsymbol{\eta}_i; \boldsymbol{u}_j, \boldsymbol{\eta}_j)^*.
$$

Thanks to the coercivity of A, it follows that $\mathcal{B}_{0,0}$ is negative definite and then (17) becomes

$$
\mathcal{B}_{G_1,G_2}(\boldsymbol{k}) = \boldsymbol{F}.
$$

Thanks to the linearity of $\mathcal{B}_{G_1,G_2}$, system (17) effectively reduces to

$$
\mathcal{B}_{0,0}(\boldsymbol{k}) = \boldsymbol{F} - \mathcal{B}_{G_1,G_2}(\boldsymbol{0})
$$

and therefore the solution $\boldsymbol{k}$ exists unique. The corresponding $[\boldsymbol{u}, p, \boldsymbol{\eta}, \boldsymbol{\beta}]$ and $[\boldsymbol{\lambda}_u, \lambda_p, \boldsymbol{\lambda}_\eta, \lambda_\beta]$ are then defined uniquely by the well posedness of problem (16) □

As pointed out in Proposition 1, the hypothesis of Proposition 2 is satisfied for a linear elastic structure coupled with a viscous fluid featuring a large enough viscosity μ.

19

In this section we detail some algorithms for the numerical solution of the coupled system (15). Resorting to iterative methods has the advantage of splitting the global problem into simpler subproblems and of possibly using standard FSI solvers. The *steepest descent method* applied for the localization of a stationary point of the Lagrange functional (14) can be equivalently thought as a Richardson method applied to equations $< d\mathcal{L}_{k_j}, \nu >= 0$, $j = 1, \ldots, m$. In this way we solve separately the two FSI problems, namely the state and the adjoint ones, and we check the optimality conditions until convergence.

Let us introduce two inf-sup compatible finite dimensional subspaces $\boldsymbol{V}_h^* \subset \boldsymbol{V}^*$ and $Q_h^* \subset Q^*$ and the finite dimensional subspace $\boldsymbol{W}_h \subset \boldsymbol{W}$. Moreover, given a quantity f, we indicate again with f its finite element approximation. In what follows, we detail three alternative algorithms.

"Exact" algorithm

The following algorithm solves the space discretization of system (15) exactly up to the error associated with the convergence test.

Algorithm 3

```
- Temporal loop
   - Internal loop: given k¹ⱼ, j = 1,...,m, and ε > 0, set l = 1 and
     do until convergence
        - Solve the numerical approximation of the state problem
          (15a), obtaining the solution uˡ, pˡ;
        - Solve the numerical approximation of the adjoint FSI problem
          (15b), obtaining the solution λˡᵤ, λˡₚ;
```

- Convergence test: if $\dfrac{|\int_{\Gamma_j^*} \boldsymbol{\lambda}_u^l \cdot \boldsymbol{n}\, d\gamma|}{|\int_{\Gamma_j^*} \boldsymbol{\lambda}_u^1 \cdot \boldsymbol{n}\, d\gamma|} < \varepsilon,\ \forall j = 1, \ldots, m$ then

```
     break;
     else   k^{l+1}_j = k^l_j + τˡ ∫_{Γ*_j} λˡᵤ · n dγ,   ∀j = 1,...,m,   and set
     l = l + 1;
   end;
end temporal loop.
```

Parameter τ^l can be chosen following different strategies. The following expression

$$\tau^l = \tau_N^l = -\frac{J_F(\boldsymbol{u}^l)}{\|\mathcal{L}_{\boldsymbol{k}}^l\|_2^2}, \tag{18}$$

stems from the application of the classical Newton method for the equation $J_F(\boldsymbol{k}) := J_F(\boldsymbol{u}(\boldsymbol{k})) = 0$. A further improvement can be obtained by observing

that J_F is a quadratic functional and the associate solution is supposed to have multiplicity 2, so that we could select $\tau^l = 2\tau_N^l$ (see [12]).

"Inexact" algorithms

Since we are not interested to the whole adjoint solution, but only in its flow rates through the sections Γ_i^*, $i = 1, \ldots, m$, we can consider an inexact solution of this problem, leading to a considerable saving of the computational cost. More precisely, we solve, out of the temporal loop, m FSI problems in the reference domain Ω_f^0, with unit Neumann conditions at Γ_j^0, $j = 1, \ldots, m$, that is

$$
\begin{cases}
A(\boldsymbol{v}, \boldsymbol{\psi}; \widetilde{\boldsymbol{\lambda}}_{u,j}, \widetilde{\boldsymbol{\lambda}}_{\eta,j})^0 + B(\widetilde{\lambda}_{p,j}; \boldsymbol{v}, \boldsymbol{\psi})^0 + C(\widetilde{\boldsymbol{\lambda}}_{\beta,j}; \boldsymbol{v}, \boldsymbol{\psi})^0 = -\int_{\Gamma_j^0} \boldsymbol{v} \cdot \boldsymbol{n} \, d\gamma \\
B(q; \widetilde{\boldsymbol{\lambda}}_{u,j}, \widetilde{\boldsymbol{\lambda}}_{\eta,j})^0 = 0 \\
C(\boldsymbol{\alpha}; \widetilde{\boldsymbol{\lambda}}_{u,j}, \widetilde{\boldsymbol{\lambda}}_{\eta,j})^0 = 0,
\end{cases}
\tag{19}
$$

$\forall \boldsymbol{v} \in \boldsymbol{V}_h^0$, $\widehat{\boldsymbol{\psi}} \in \boldsymbol{W}_h$ and $q \in Q_h^0$. Then, at each internal iteration of Algorithm 3 we combine linearly these solutions, obtaining

$$
\boldsymbol{\lambda}_u = \sum_{j=1}^m \left(\int_{\Gamma_j^*} \boldsymbol{u} \cdot \boldsymbol{n} \, d\gamma - F_j \right) \boldsymbol{\lambda}_{u,j},
\tag{20}
$$

where the $\boldsymbol{\lambda}_{u,j}$'s are obtained from $\widetilde{\boldsymbol{\lambda}}_{u,j}$ through the ALE map. This introduces an approximation error in the construction of the adjoint problem, since we are combining solutions obtained in the fixed reference frame.

In what follows, we detail two possible inexact algorithms. If we choose a monolithic strategy for the treatment of interface conditions, the only quantities updated in the inner loop in Algorithms 3 are the control variables k_j, $j = 1, \ldots, m$. Otherwise, if we use a partitioned procedure we need to subiterate also on the interface position between the fluid and the structure subproblems. In this case, we can consider either "nested iterations" or just "one loop". In particular, we detail for the sake of exposition the case in which the Dirichlet-Neumann scheme is used for the treatment of the interface conditions. However, extension to general Robin-Robin schems is straightforward.

Algorithm 4 *: Inexact Nested Loops*

   - Solve for each $i = 1, \ldots, m$ the numerical approximations of the
     FSI problems (19), obtaining, in particular, the velocities $\widetilde{\boldsymbol{\lambda}}_{u,j}$;
   - Temporal loop;
     - ``Control variables'' loop (index l): given k_j^1, $j = 1, \ldots, m$
       and $\varepsilon_2 > 0$, set $l = 1$ and do until convergence
        - ``Interface condition'' loop (index p): given $\boldsymbol{\eta}_p^l$ and $\varepsilon_1 >$

0, solve in sequence until convergence

- A Fluid subproblem with the following boundary conditions

$$\boldsymbol{u}^l_{p+1} = \frac{\boldsymbol{\eta}^l_p - \boldsymbol{\eta}^n}{\Delta t} \qquad \text{on } \Sigma^*$$

$$\boldsymbol{T}^l_{f,p+1}\boldsymbol{n} = k^l_j \boldsymbol{n} \qquad \text{on } \Gamma^*_j, \quad j = 1, \ldots, m;$$

- A Structure subproblem with the following boundary condition

$$\boldsymbol{T}^l_{s,p+1}\,\boldsymbol{n} = \boldsymbol{T}^l_{f,p+1}\,\boldsymbol{n} \quad \text{on } \Sigma^*;$$

  - Convergence test: if

$$\|\boldsymbol{u}^l_{p+1} - \boldsymbol{u}^l_p\|_{L^2(\Sigma^*)} < \varepsilon_1, \tag{21}$$

then break;
  - end ''interface conditions'' loop;
- Compute the approximate adjoint solution with (20);
- Convergence test: if

$$\frac{|\int_{\Gamma^*_j} \boldsymbol{\lambda}^l_{u,h} \cdot \boldsymbol{n}\, d\gamma|}{|\int_{\Gamma^*_j} \boldsymbol{\lambda}^1_{u,h} \cdot \boldsymbol{n}\, d\gamma|} < \varepsilon_2, \ \forall j = 1, \ldots, m \tag{22}$$

then break;
else

$$k^{l+1}_{j,h} = k^l_{j,h} + \tau^l \int_{\Gamma^*_j} \boldsymbol{\lambda}^l_{u,h} \cdot \boldsymbol{n}\, d\gamma, \quad \forall j = 1, \ldots, m, \tag{23}$$

and set $l = l + 1$;
  - end ''control variables'' loop;
- end temporal loop.

Algorithm 5 : *Inexact One Loop*

- Solve for each $i = 1, \ldots, m$ the numerical approximations of the FSI problems (19), obtaining, in particular, the velocities $\widetilde{\boldsymbol{\lambda}}_{u,j}$;
- Temporal loop;
  - ''Control variables'' and ''Interface condition'' loop (index l): given k^1_j, $j = 1, \ldots, m$ and $\varepsilon_1 > 0$ and $\varepsilon_2 > 0$, set $l = 1$ and solve until convergence
    - A Fluid subproblem with the following boundary conditions

$$\boldsymbol{u}^l = \frac{\boldsymbol{\eta}^{l-1} - \boldsymbol{\eta}^n}{\Delta t} \qquad \text{on } \Sigma^*$$

$$\boldsymbol{T}^l_f \boldsymbol{n} = k^l_j \boldsymbol{n} \qquad \text{on } \Gamma^*_j, \quad j = 1, \ldots, m;$$

22
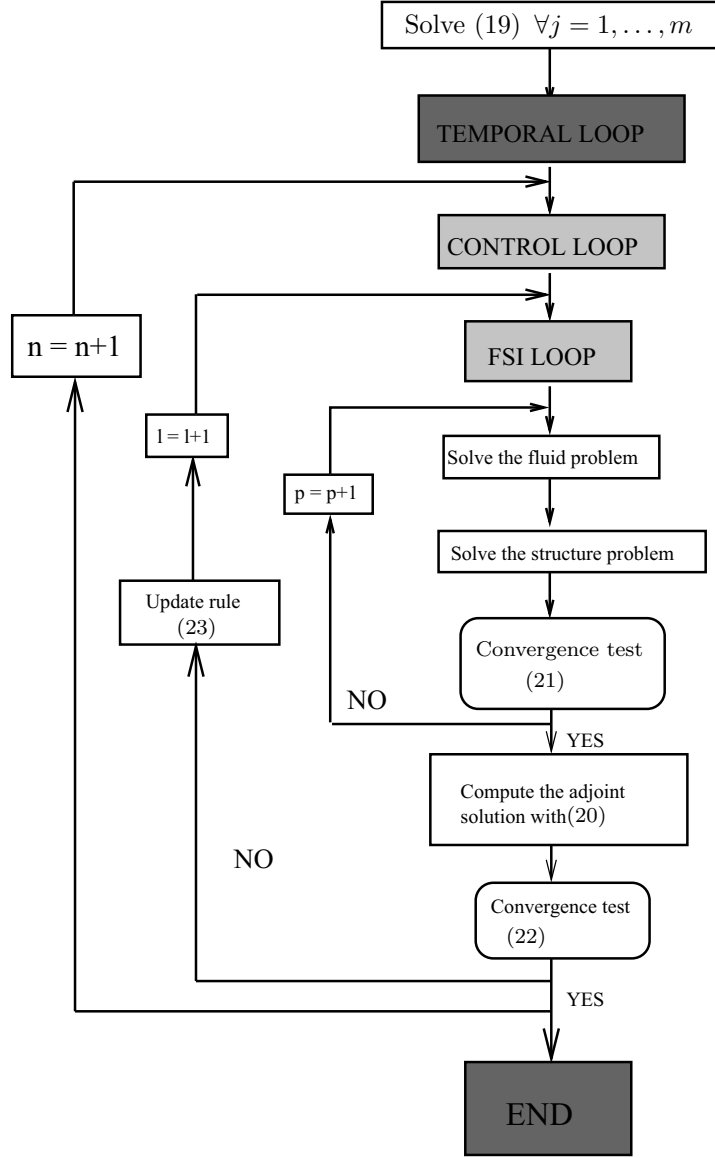
Fig. 3. Scheme of Algorithm 4.

- A Structure subproblem with the following boundary condition

$$\boldsymbol{T}_s^l\,\boldsymbol{n} = \boldsymbol{T}_f^l\,\boldsymbol{n} \quad \text{on } \Sigma^*;$$

- Compute the approximate adjoint solution with (20);
- Convergence test: if

$$\|\boldsymbol{u}^l - \boldsymbol{u}^{l-1}\|_{L^2(\Sigma^*)} < \varepsilon_1 \quad \text{and} \quad \frac{|\int_{\Gamma_j^*} \boldsymbol{\lambda}_{u,h}^l \cdot \boldsymbol{n}\,d\gamma|}{|\int_{\Gamma_j^*} \boldsymbol{\lambda}_{u,h}^1 \cdot \boldsymbol{n}\,d\gamma|} < \varepsilon_2, \ \forall j = 1, \ldots, m$$

then break;
else $\quad k_{j,h}^{l+1} = k_{j,h}^l + \tau^l \int_{\Gamma_j^*} \boldsymbol{\lambda}_{u,h}^l \cdot \boldsymbol{n}\,d\gamma, \quad \forall j = 1, \ldots, m, \quad$ and set $\quad l =$

```
      l + 1;
    - end ``control variables'' and ``interface conditions'' loop;
  - end temporal loop.
```
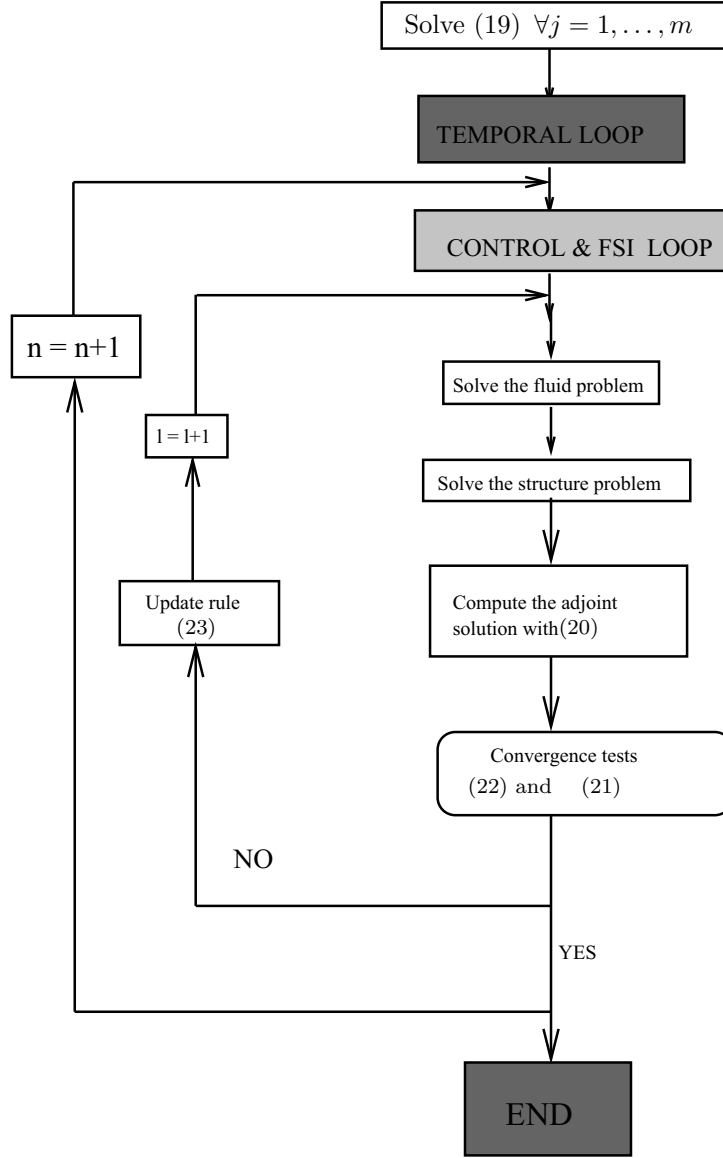

Fig. 4. Scheme of Algorithm 5.

Obviously, for Alg. 5 the convergence is not guaranteed, since at each subiteration the interface conditions are not satisfied exactly. However, the numerical results presented in Sect. 6, show that at least for the cases treated in this work, convergence is always achieved.

In Fig. 3 and 4 schemes of Algorithms 4 and 5 are reported.

Remark 3 *In all the three strategies proposed in Sect. 3, 4 and 5, in fact the flow rate at an artificial section Γ is prescribed by forcing an appropriate*

unknown constant normal stress on Γ. As observed in [13,17,12], when the transpose formulation of the diffusion term is considered, namely $\mu(\nabla \boldsymbol{u} + (\nabla \boldsymbol{u})^T)$, the solution is affected by a spurious tangential velocity $\boldsymbol{u}_{sp}^\tau$ at Γ. In the rigid case, this drawback can be overcome by imposing directly that the tangential velocity $\boldsymbol{u}^\tau = \boldsymbol{u}_{sp}^\tau$ is equal to zero (see [17]) or by resorting to the minimization of a suitable functional (see [12]). However, in the compliant case the tangential velocity on Γ is given by two contributions, namely $\boldsymbol{u}^\tau = \boldsymbol{u}_{sp}^\tau + \boldsymbol{u}_\eta^\tau$, where the latter term is due to the displacement of the FS interface. Numerical strategies for the separation of the two contribution in order to skip the spurious one are under investigation. However, numerical evidences show that, for the problems considered in this work, the contribution of $\boldsymbol{u}_{sp}^\tau$ is only of about 1% of the total tangential velocity $\boldsymbol{u}^\tau$, so it is supposed to play a minor role in numerical simulations.

6 Numerical results

In this section we present some numerical results with the aim of testing the algorithms proposed in the previous sections. In all the simulations, we have considered a *semi-implicit* treatment of the interface position.

6.1 Comparison among the various algorithms

In the first set of simulations we test the performances of Algorithms 1, 2, 3, 4 and 5 in terms of number of iterations and CPU times. The numerical simulations are performed in a rectangular domain both for the fluid and for the two structures, whose size is $6 \times 1\,cm$ and $6 \times 0.1\,cm$, respectively (see Fig. 5). For the structure, we consider the following equation of linear elasticity
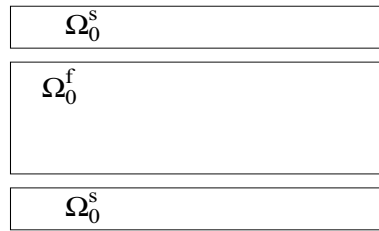

Fig. 5. Computational fluid and structure domains.

$$\rho_s \partial_{tt}\boldsymbol{\eta} - c\nabla \cdot (\nabla\boldsymbol{\eta} + (\nabla\boldsymbol{\eta})^t) - \lambda\nabla \cdot ((\nabla \cdot \boldsymbol{\eta})I) + \beta\boldsymbol{\eta} = \boldsymbol{0},$$

where I is the identity operator, $c = E/(1 + \nu)$, $\lambda = \nu E/((1 + \nu)(1 - 2\nu))$ and $\beta = E/(1 - \nu^2)R^2$, with E the Young modulus, ν the Poisson ratio and R the radius of the fluid domain. The reaction term stands for the transversal

membrane effects. We prescribe the flow rate $F = \cos(2\pi t)$ at the inlet of the fluid domain.

We use a 2D Finite Element Code written in Matlab at MOX - Dipartimento di Matematica - Politecnico di Milano and at CMCS - EPFL - Lausanne. We consider $\mathbb{P}_1 - bubble/\mathbb{P}_1$ elements for the fluid and $\mathbb{P}_1$ element for the structure and a space discretization step $h = 0.02\,cm$. Moreover, we set $\mu = 0.035\,cm^2/s$ and $\rho_f = 1\,g/cm^2$ and, unless otherwise specified, we consider the following reference values: $\Delta t = 10^{-2}s, \rho_s = 1.1\,g/cm^2$, $c = 1.15 \cdot 10^6\,dyne$, $\lambda = 1.7 \cdot 10^6\,dyne$, $\beta = 6.5 \cdot 10^5\,dyne/cm^2$ and the thickness of the structure $H_s = 0.1\,cm$.

For all the algorithms a Robin-Neumann partitioned procedure is used for the solution of the FSI problems, with a stopping criterion based on the normalized residual (see [3]) and tolerance equal to 10^{-4}. For Algorithms 3 and 4, the tollerance for the stopping criterion in the control loop is set equal again to 10^{-4}. For Algorithm 5 we have only one tollerance, set again equal to 10^{-4}.

In Fig. 6 the fluid axial velocity at the inlet of the domain at two different instants obtained with Algorithms 1, 2 and 3 is shown. The solution obtained with the inexact Algorithms 4 and 5 are not reported since they are in excellent agreement with the solution obtained with Alg. 3.
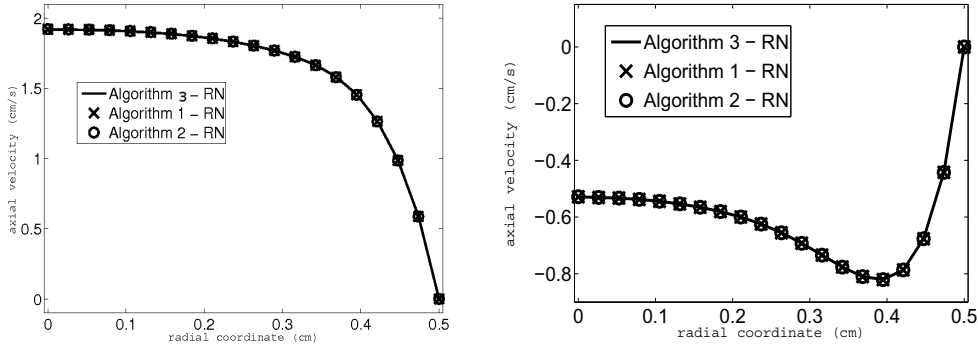

Fig. 6. Comparison of axial velocities obtained with Algorithms 1, 2 and 3. - $t = 0.10\,s$ (left), $t = 0.30\,s$ (right) .

In Tab. 1, the left value in each box is the mean number of total iterations per time step. In particular, for Algorithm 2 we reported the sum of the mean number of Robin-Neumann iterations needed to solve the first and the second FSI problem in the GMRes loop. For Algorithm 1 each of the RN iterations is a flow rate problem which has been solved with the GSC (rigid) scheme, requiring the solution of two fluid problems. For what concerns Algorithms 3 and 4, the mean number of iterations per time step of the control loop multiplied for the mean number of iterations of the Robin-Neumann scheme per control loop's iteration, is reported. For Algorithm 5 the mean number of

26

iterations per time step refers to the unique loop. On the right of each block the CPU time to perform 10 time steps, normalized with the best performance, is shown.

	Alg. 1	Alg. 2	Alg. 3	Alg. 4	Alg. 5
$\beta,\ \Delta t,\ \rho_s$	$9.1 - 1.00$	$11.4 - 1.24$	$3 \times 7.6 - 2.46$	$3 \times 5.9 - 1.96$	$11.6 - 1.32$
$10\beta,\ \Delta t,\ \rho_s$	$4.7 - 1.00$	X	$3 \times 4.0 - 2.49$	$3 \times 3 - 1.91$	$5.2 - 1.16$
$\beta,\ \Delta t/10,\ \rho_s$	$21.9 - 1.04$	$28.1 - 1.34$	$3 \times 18.2 - 2.60$	$3 \times 13.5 - 1.99$	$19.4 - 1.00$
$\beta,\ \Delta t,\ 10\rho_s$	$8.4 - 1.00$	$10.8 - 1.26$	$3 \times 7.4 - 2.58$	$3 \times 5.7 - 2.05$	$11.4 - 1.39$

Table 1

Mean number of iterations per time step (left) and relative CPU time in seconds to perform 10 time steps (right). X means that convergence is not achieved.

Let us discuss the results in Tab. 1 starting from the three algorithms for the solution of system (15), namely Alg. 3, 4 and Alg. 5 . First of all, we point out that both the inexact algorithms 4 and 5 converge in all the numerical simulations. A convergence analysis of such schemes is still missing. However, these experimental results are very promising. Among these three schems, Alg. 5 seems to be the most performing. Indeed, the (mean) reduction factor of the CPU times is 2.08 with respect to Alg. 3 and 1.61 with respect to Alg. 4. Therefore, the use of just one loop seems to be the most promising and then only Algorithm 5 is considered in the sequel.

Let us now focus on Alg. 1, 2 and 5. We observe that Alg. 1 is the most performing in all cases but one, that is for a small value of the time discretization, where Alg. 5 is faster. Alg. 2 works quite well for big values of Δt and β and does not converge for a value of β equal to 10 times the reference value. All the algorithms seems to be insensitive to an increment of the structure density. This is due to the choice of the Robin-Neumann scheme as partitioned procedures, which has been shown to be robust with respect to the added mass effect (see [3]).

6.2   An application to a 2D bifurcation geometry

In this section we apply Alg. 1 and 5 to a 2D geometry which is an idealization of a realistic domain, namely the human carotid. We use the same parameters introduced in the previous subsection, apart for the values $\beta = 1.3 \cdot 10^6 dyne/cm^2$ and $\Delta t = 10^{-3}s$. We impose the following flow-rate impulse

$$F(t) = \begin{cases} F_{in} \ t \leq 0.005\,s \\ 0 \quad t > 0.005\,s \end{cases}$$

27

and we use the Robin-Neumann scheme as partitioned procedure. In Fig. 7 the pressure in the deformed fluid domain and the exploded position of the structure obtained with Alg. 5 are shown at 4 different instants. The flow-rate impulse is $F_{in} = 50\,cm^2/s$. The solutions obtained with Alg. 1 are in excellent agreement and for this reason their visualization are not reported. In Tab. 2 the mean number of iterations (left) and the CPU times normalized
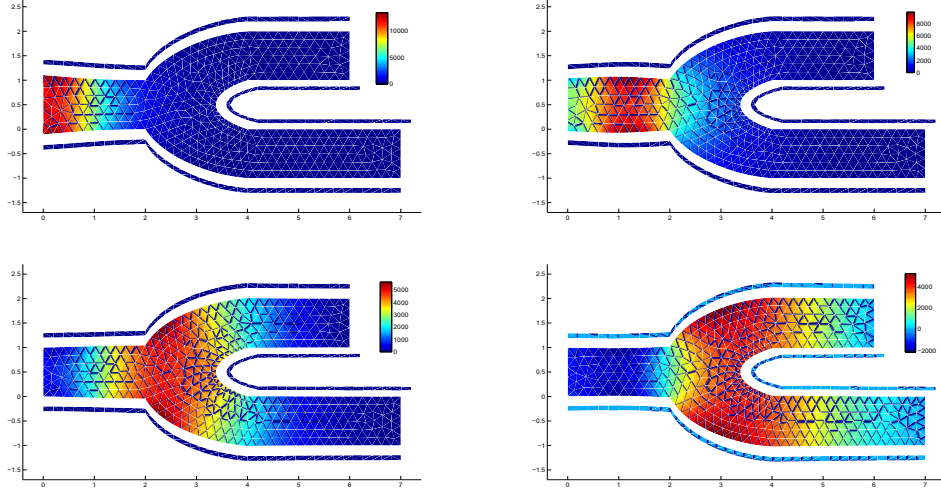

Fig. 7. Pressure in the deformed fluid domain and position of the structure obtained with Alg. 5 - $t = 0.004$ (up-left), $t = 0.008\,s$ (up-right), $t = 0.012\,s$ (bottom-left) and $t = 0.016\,s$ (bottom-right).

with the best performance (right) are reported for 2 values of the flow-rate impulse, namely $F_{in} = 10\,cm^2/s$ and $F_{in} = 50\,cm^2/s$. We point out that the

	Alg. 5	Alg. 1
$F_{in} = 10\,cm^2$	$14.2 - 1.00$	$20.25 - 1.37$
$F_{in} = 50\,cm^2$	$14.3 - 1.00$	$19.9 - 1.39$

Table 2
Mean number of iterations per time step (left) and relative CPU time in seconds (right) to perform 16 time steps for the carotid simulation.

computational effort of the two algorithms seems to be independent of the Reynolds number. However, Alg. 5 performs better than Alg. 1, both in term of number of subiterations needed to reach convergence and of CPU time.

7   Conclusions

In this paper we focus on the problem arising when the fluid-structure interaction (FSI) problem is solved in a truncated computational domain, in

particular when no sufficient data are available to be prescribed at the artificial sections. Among the varoius "defective" data, we consider here the *flow rate* conditions for the fluid. This paper has to be intended as a first step in the direction of solving a FSI problem with general fluid and structure defective data. We propose three different strategies for the numerical solution of the Flow rate/FSI problem. Among the various algorithms proposed for the numerical solution, the numerical results have showed that Alg. 5 seems to be the most suited for realistic simulations. Moreover, its versatility is very attractive when other defective data (such as the ones related to the structure) are considered. Indeed, the inclusion of these defective informations through the enrichment of the functional to be minimized should not increase the computational cost if just "one loop" implementation is used, contrary to the other strategies.

Acknowledgements

References

[1] I. Babuŝka. The finite element method with Lagrange multipliers. *Numerische Mathematik*, 20:179–192, 1973.

[2] S. Badia, F. Nobile, and C. Vergara. Robin-Robin preconditioned Krylov methods for fluid-structure interaction problems. *Submitted*.

[3] S. Badia, F. Nobile, and C. Vergara. Fluid-structure partitioned procedures based on Robin transmission conditions. *Journal of Computational Physics*, 227:7027–7051, 2008.

[4] S. Badia, A. Quaini, and A. Quarteroni. Splitting methods based on algebraic factorization for fluid-structure interaction. *SIAM Journal on Scientific Computing*, 30(4):1778–1805, 2008.

[5] M. Bernadou. *Méthodes d'Éléments Finis pour les Problèmes de Coques Minces*. Masson, 1994.

[6] D. Braess. *Finite Element*. Cambridge University Press, 2002.

[7] F. Brezzi. On the existence, uniqueness and approximation of saddle point problems arising from Lagrange multipliers. *RAIRO Anal. Numer.*, 8:129–151, 1974.

[8] J. Donea. An arbitrary Lagrangian-Eulerian finite element method for transient dynamic fluid-structure interaction. *Computer Methods in Applied Mechanics and Engineering*, 33:689–723, 1982.

[9] M.A. Fernández, J.F. Gerbeau, and C. Grandmont. A projection semi-implicit scheme for the coupling of an elastic structure with an incompressible fluid. *International Journal for Numerical Methods in Engineering*, 69(4):794–821, 2007.

[10] L. Formaggia, J.-F. Gerbeau, F. Nobile, and A. Quarteroni. Numerical treatment of defective boundary conditions for the Navier-Stokes equation. *SIAM Journal on Numerical Analysis*, 40(1):376–401, 2002.

[11] L. Formaggia, A. Quarteroni, and A. Veneziani (Eds.). *Cardiovascular Mathematics - Modeling and simulation of the circulatory system.* Springer, 2009.

[12] L. Formaggia, A. Veneziani, and C. Vergara. A new approach to numerical solution of defective boundary value problems in incompressible fluid dynamics. *SIAM Journal on Numerical Analysis*, 46(6):2769–2794, 2008.

[13] J.G. Heywood and R. Rannacher. Finite element approximation of the nonstationary Navier-Stokes problem. I: Regularity of solutions and second-order error estimates for spatial discretization. *SIAM Journal on Numerical Analysis*, 19:275–311, 1982.

[14] J.G. Heywood, R. Rannacher, and S. Turek. Artificial boundaries and flux and pressure conditions for the incompressible Navier-Stokes equations. *International Journal for Numerical Methods in Fluids*, 22:325–352, 1996.

[15] T. J. R. Hughes, W. K. Liu, and T. K. Zimmermann. Lagrangian-Eulerian finite element formulation for incompressible viscous flows. *Computer Methods in Applied Mechanics and Engineering*, 29(3):329–349, 1981.

[16] F. Nobile and C. Vergara. An effective fluid-structure interaction formulation for vascular dynamics by generalized Robin conditions. *SIAM Journal on Scientific Computing*, 30(2):731–763, 2008.

[17] A. Veneziani. *Mathematical and numerical modeling of blood flow problems.* PhD thesis, University of Milano, 1998.

[18] A. Veneziani and C. Vergara. Flow rate defective boundary conditions in haemodinamics simulations. *International Journal for Numerical Methods in Fluids*, 47:803–816, 2005.

[19] A. Veneziani and C. Vergara. An approximate method for solving incompressible Navier-Stokes problems with flow rate conditions. *Computer Methods in Applied Mechanics and Engineering*, 196(9-12):1685–1700, 2007.